INL/RPT-23-72874

Overlapping Domain Coupling of Multidimensional and System Codes in NEAMS - Pronghorn and SAM

May 2023

Nuclear Energy Advanced Modeling and Simulation M2 Milestone

Sebastian Schunert[1], Mauricio Tano Retamales[1], and Mustafa Jaradat[1]

[1]*Idaho National Laboratory*

Idaho National Laboratory

INL is a U.S. Department of Energy National Laboratory operated by Battelle Energy Alliance, LLC

INL/RPT-23-72874

Overlapping Domain Coupling of Multidimensional and System Codes in NEAMS - Pronghorn and SAM

Nuclear Energy Advanced Modeling and Simulation M2 Milestone

Sebastian Schunert[1], **Mauricio Tano Retamales**[1], **and Mustafa Jaradat**[1]

[1]**Idaho National Laboratory**

May 2023

Idaho National Laboratory
Idaho Falls, Idaho 83415

http://www.inl.gov

Prepared for the
U.S. Department of Energy
Office of _____
Under DOE Idaho Operations Office
Contract DE-AC07-05ID14517

Page intentionally left blank

ABSTRACT

This report describes the implementation and testing of domain-overlapping coupling of the Pronghorn and SAM codes. Both Pronghorn and SAM are codes developed by the DOE Nuclear Energy Advanced Modeling and Simulation (NEAMS) program for analysis of advanced nuclear reactors. Pronghorn focuses on analyzing multi-dimensional core flow conditions, while SAM focuses on analysis of the entire system including, among other components, piping, pumps, and heat exchangers. It is desirable for many advanced reactor thermal-hydraulics simulations to couple Pronghorn and SAM to obtain self-consistent solutions in the core and the system. The domain-overlapping coupling approach provides a robust and numerically efficient candidate for this coupling. We describe the algorithm for obtaining self-consistent solutions between a SAM network of flow channels and an overlapped multi-dimensional Pronghorn domain. The algorithm is tested for a variety of simple canonical test problems and a model of the Molten Salt Reactor Experiment (MSRE). Results demonstrate that the domain overlapping coupling approach provides consistent pressure, mass flow rate, enthalpy, and passive scalar distributions between Pronghorn and SAM and converges reliably and efficiently (at most 15 iterations, usually much less than 10) for the considered test problems.

Page intentionally left blank

CONTENTS

FIGURES

TABLES

ACRONYMS

CFD	Computational Fluid Dynamics
FHR	Fluoride-Salt-Cooled High-Temperature Reactor
FV	finite volume
MOOSE	Multiphysics Object-Oriented Simulation Environment
MSR	Molten Salt Reactor
MSRE	Molten Salt Reactor Experiment
NEAMS	Nuclear Energy Advanced Modeling and Simulation

Page intentionally left blank

1. Introduction

This report describes the implementation and testing of domain-overlapping coupling of the Pronghorn and SAM codes. Both Pronghorn and SAM are codes developed by the DOE Nuclear Energy Advanced Modeling and Simulation (NEAMS) program for analysis of advanced nuclear reactors. Pronghorn focuses on analyzing multi-dimensional core flow conditions, while SAM focuses on analysis of the entire system including, among other components, piping, pumps, and heat exchangers. It is desirable for many advanced reactor thermal-hydraulics simulations to couple Pronghorn and SAM to obtain self-consistent solutions in the core and the system. The domain-overlapping coupling approach provides a robust and numerically efficient candidate for this coupling. We describe the algorithm for obtaining self-consistent solutions between a SAM network of flow channels and an overlapped multi-dimensional Pronghorn domain. The algorithm is tested for a variety of simple canonical test problems and a model of the Molten Salt Reactor Experiment (MSRE).

Pronghorn [1] is a Multiphysics Object-Oriented Simulation Environment (MOOSE) [2] based multi-dimensional, thermal-hydraulics core simulator for the analysis of advanced reactors. It implements approaches that are less accurate than Computational Fluid Dynamics (CFD), but allow multi-dimensional, transient analysis of reactor cores on desktop computers. For this purpose, Pronghorn implements engineering scale algorithms such as porous flow and subchannel methods [3]. The subchannel method [4] is made available by a separate code package [5, 6] under MOOSE that is organized as git submodule of Pronghorn. Pronghorn uses MOOSE's finite volume (FV) capabilities for discretizing the balance equations for mass, momentum, energy, and passive scalars [7].

The System Analysis Module (SAM) is [8] "an advanced and modern system analysis tool under development at Argonne National Laboratory for advanced non-LWR reactor safety analysis. It aims to provide fast-running, modest-fidelity, whole-plant transient analyses capabilities, which are essential for fast turnaround design scoping and engineering analyses of advanced reactor concepts. [...] SAM aims to be a generic system-level safety analysis tool for advanced non-LWRs, including Liquid-Metal-cooled fast Reactors (LMR), Molten Salt Reactors (MSR), Fluoride-salt-cooled High- temperature Reactors (FHR), and High-Temperature

Gas-cooled Reactors (HTGR). SAM takes advantage of advances in physical modeling, numerical methods, and software engineering to enhance its user experience and usability. It utilizes an object-oriented computational framework (MOOSE), and its underlying meshing and finite-element library and linear and non-linear solvers, to leverage the modern advanced software environments and numerical methods."

Coupling thermal-hydraulics core and system capabilities is important for NEAMS for a wide variety of applications. A selection of these applications is:

- Steady-state conditions of reactor core flow conditions.
- All transients that are caused or influenced by the interaction of the primary and secondary system.
- Steam or air ingress for gas-cooled reactors.
- Pressurized loss of forced cooling in gas-cooled reactors where natural circulation in the system and natural convection in the core interact. Note that in this case, a flow reversal from top-bottom to bottom-top occurs.
- Loss of flow conditions in Fluoride-Salt-Cooled High-Temperature Reactors (FHRs) where natural circulation in the system and natural convection in the core interact.
- Molten Salt Reactors (MSRs) where decay of neutron precursors in the primary system is important, but the core thermal-hydraulics is multi-dimensional.

We adopt domain overlapping coupling between the thermal-hydraulic core simulator and the system code. Domain-overlapping coupling can be implemented in MOOSE within a reasonable time frame because its coupling paradigm works well with MOOSE's *MultiApp* system [9]. Domain-segregated coupling where only boundary conditions are exchanged between the codes may converge slowly or not converge [10–12]. The domain-overlapping approach was selected after promising progress was reported by a different research team coupling nekRS and SAM [11, 12]. The algorithms reported in this work are based on this earlier work, but in some instances different choices were made. These differences will be pointed out in the report.

An important requirement driving this work was the usability of the domain-overlapping capability. MOOSE supports flexible composition of problems including both different iteration

and communication schemes between Pronghorn and SAM. However, as the complexity of the problem grows, so does the complexity of the input. For moderately complex problems, the input files are not reasonably maintainable. Therefore, a core component of this work is the development of a custom action that sets up the MOOSE simulation with a minimum of user input.

2. Theory

2.1 Requirements for the Pronghorn-SAM Coupling Algorithm

The domain-overlapping coupling between Pronghorn and SAM must satisfy the following requirement:

- Numerically stable for a wide range of typical problems.
- Reasonably fast convergence of the fixed-point iterations between Pronghorn and SAM.
- Support multiple boundaries (i.e. more than 2) on the Pronghorn domain.
- Allow reversal of flow over boundaries (i.e., an inlet becomes an outlet or vice versa).
- Support an arbitrary number of passively advected scalar variables.
- Support compressible fluids.
- Support natural circulation.
- Must be capable of computing self-consistent solutions between Pronghorn and SAM.

A solution is self-consistent if the values of the mass flow rates, pressures, enthalpies, and passive scalars are identical at the boundary in Pronghorn and SAM.

2.2 Topology of the Overlapped SAM Components

A sufficiently general problem is depicted in Fig. 1. In this figure, the blue shaded area is the Pronghorn domain with 5 boundaries labeled $\{E_i\}_{i=1,..,5}$. Overlapped SAM components are indicated in red and labeled $\{C_i\}_{i=1,..,5}$; all $\{C_i\}_{i=1,..,5}$ are connected to a common branch. SAM components that are on the outside of the overlapped region are indicated in black and are not labeled.

It is important to establish that the overlapped components $\{C_i\}_{i=1,..,5}$ do not have to produce physically accurate representation of the distribution of quantities of interest (pressure, velocity, temperature, passive scalars) with the exception for the values on the boundaries $\{E_i\}_{i=1,..,5}$. The

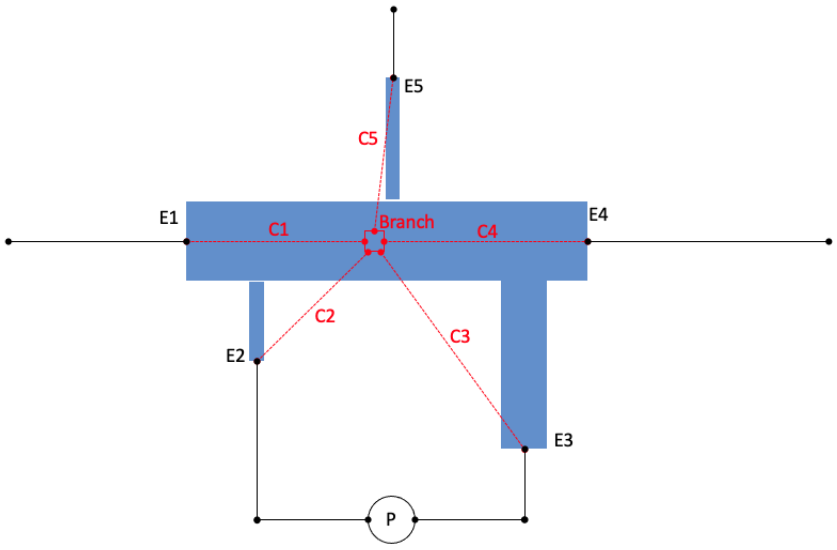

Figure 1: Conceptual sketch of a multi-dimensional flow domain with the overlaid system code structure.

overlapped components $\{C_i\}_{i=1,..,5}$ merely exist to facilitate convergence between the Pronghorn and SAM problems.

The topology depicted in Fig. 1 satisfies all the requirements stated in Sect. 2.1. Each boundary in the multi-dimensional domain, E_i, is paired with a single *PBOneDFluidComponent*, C_i. All C_i are connected to a single branch. This topology provides enough degrees of freedom in the form of adjustable "source terms" to match all relevant quantities (average/integral pressure, mass flow rates, temperatures, advected scalars) on all boundaries E_i. Again, the value of these quantities along the extent of the components or in the branch has no physical connection with any of the values encountered in the multi-dimensional problem.

It is convenient to introduce some nomenclature for future reference in this report. The end of the flow component C_i that faces the boundary E_i is referred to as the system side of component C_i, while the side that faces the common branch is the branch side. Within SAM, a *PBOneDFluidComponent* has two boundaries labeled (in) and (out) with the former located at the spatial position set by the *position* parameter and the latter located at the other end (*position* plus length times the *orientation* parameter). The pipe's orientation thus always points from (in) to (out). There are two different ways on how to orient the overlapped components with respect to the topology in Fig. 1: first, (in) can be located on the system side, and second, (in) can be located

on the branch side. In the first case, we refer to the component to be oriented *inward*, while it is oriented *outward* in the second case.

We adopt the convention that velocities and mass flow rates flowing into the overlapped region is positive and velocities and mass flow rates flowing out of the overlapped region are negative. This is in contrast to the SAM convention, where flow in the direction of the component's orientation is positive. The appropriate conversions are performed when information is transferred between Pronghorn and SAM.

2.3 Numerical Algorithms

In this section, the numerical algorithms to obtain a self-consistent solution between Pronghorn and SAM are introduced.

2.4 Nomenclature and Notation

We begin by defining nomenclature and notation that is useful for the exposition of the overlapping domain coupling algorithm. All Pronghorn quantities are denoted as capital letters (e.g. $\vec{V}$ for the velocity, P for the pressure, Θ for temperature, etc), while SAM quantities are denoted in lower case letters (e.g. $\vec{v}$ for the velocity, p for the pressure, θ for temperature, etc). The exception to this rule is the density because the uppercase version is identical to P; therefore, SAM density is denoted by ρ and Pronghorn density is denoted by ϱ.

Mass-flux weighted averages over boundary E_i of an arbitrary quantity F are denoted by:

$$\langle F \rangle_{E_i} = \frac{\int_{E_i} F \varrho \vec{V} \cdot \vec{n} dS}{\int_{E_i} \varrho \vec{V} \cdot \vec{n} dS}, \tag{1}$$

where $\vec{n}$ is the normal vector. Standard averages over a surface are denoted by:

$$\overline{F}_{E_i} = \frac{\int_{E_i} F dS}{\int_{E_i} dS}, \tag{2}$$

Fixed point iteration indices are denoted as superscript (n) with parenthesis, e.g. for pressure $P^{(n)}$. We do not indicate the time step index, but it is assumed that the iteration between Pronghorn and SAM happens within a transient execution and the solution of the last time step is used as

initial guess for the first fixed point iteration of the current time step.

SAM quantities evaluated at the system side boundary of component i are denoted by subscripts E, i, while quantities evaluated at the branch side are denoted by subscript B, i. Volumetric quantities like the distributed friction factor, heat source, and passive scalar source get a single subscript index i indicating which component they are associated with. Quantities in the branch themselves are denoted by subscript B.

The geometric parameters of the flow channel are its length L_i, hydraulic diameter $D_{H,i}$, and constant flow area A_i. The flow area should be set to match the area of the boundary E_i.

2.5 Iteration between Pronghorn and SAM and Information Transfer

An overview of the iteration and information transfers between Pronghorn and SAM is depicted in Fig. 2. At each time step, a fixed point iteration with alternating solves on SAM and then Pronghorn is performed. The initial guess for the first fixed point iteration per time step is provided by the last iterate of the last time step. Information are transferred from Pronghorn to SAM before the SAM solve (P-to-S) and from SAM to Pronghorn before the Pronghorn solve (S-to-P).

The described algorithm uses only adjustable volumetric source terms[1] to match the variables of interest (pressure, mass flow rate, enthalpy, passive scalars) computed by Pronghorn and SAM at the system side boundaries E_i. The P-to-S information transfer communicates these sources to SAM. The sources are:

- the friction factor f_i for each component.
- the distributed heat source $\dot{q}_i$ for each component.
- a distributed source of the passive scalar $s_{i,k}$ for each component and passive scalar indicated by k.

These quantities are transferred as *Postprocessors* and then provided to SAM components as *ParsedFunction*. The computation of f_i, $\dot{q}_i$, and $s_{i,k}$ is described in detail in Sect. 2.6.

The S-to-P information transfer communicates the following quantities to Pronghorn:

[1] In the case of matching pressure drops, we use a friction factor which is not a traditional externally imposed source.

- The pressure in the branch, p_B; the component pressures at all branch and system side boundaries $p_{B,i}$, $p_{E,i}$.
- The density at all branch and system side boundaries $\rho_{B,i}$, $\rho_{E,i}$.
- The mass flow rate at the system side boundary $\dot{m}_{E,i}$. We use the convention in this report and in the implementation that flow into the overlapped region is positive (i.e. flow from the system to the branch side).
- (if energy equation is present) the boundary temperatures $\theta_{E,i}$ (these are used only on inflow boundary conditions in Pronghorn) and $\dot{h}_i = -\left(\dot{m}_{E,i} h_{E,i} - \dot{m}_{B,i} h_{B,i}\right)$.
- (if passive scalar variables are present) the values of the passive scalar variables at the system and branch side boundaries, $\phi_{E,i,k}$ and $\phi_{B,i,k}$. Note that the passive scalar transport equations in Pronghorn and SAM use definitions of the scalar variables that differ by a factor of density. We will not include the factor of density explicitly in the source term update equations developed in Sect. 2.6, because the code immediately adjusts for the difference in the transfers.

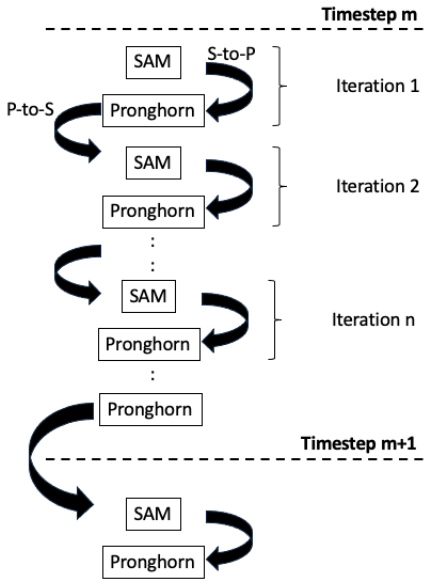

Figure 2: Fixed point iteration and data transfer strategy between Pronghorn and SAM.

2.6 Computation of the Source Terms

The domain overlapping coupling algorithm implements two different approaches to computing source terms. The *simple* approach uses only values computed on the Pronghorn side to set the sources, while the *update* approach uses the difference between component pressure drops, enthalpy balances, and passive scalar advection balances to iteratively update the respective sources in the SAM components driving the difference between Pronghorn and SAM component pressure drops, enthalpy balances, and passive scalar advection balances to zero. Only the *update* approach requires fixed-point iterations per time step.

The *simple* approach is provided as a means to create reasonable initial guesses for the *update* approach. Given poorly chosen initial conditions, the *update* approach can fail to converge so it is recommended to first iterate into a steady-state using the *simple* approach and then switch to the *update* approach. This is supported in the code by providing a time at which this switch occurs.

The *simple* approach usually does not lead to self-consistent Pronghorn and SAM solutions, especially in transient simulations and if the density varies. This will be demonstrated for the example of pressure drops during a ramping up of inlet velocity in a pipe.

2.6.1 The *simple* approach

The pressure drop in each component is controlled using the Darcy-Weisbach friction factor f_i that can be provided as *Postprocessor* to SAM components. The Darcy-Weisbach relation using SAM flow conditions is given by:

$$\Delta p_i = d(p_{E,i} - p_{B,i}) = \frac{f_i L_i}{2 D_{H,i} A_i^2} \dot{m}_i \dot{v}_i, \tag{3}$$

where $\dot{v}_i$ is the volumetric flow rate in the SAM component and $d = 1$ if the flow in the component i is from the branch to the system side and -1 if the flow is from the system side to the branch. For variable density, Eq. 3 only holds for sufficiently small sections of the flow channel's length.

The Darcy-Weisbach relation is solved for f_i, but Δp_i, $\dot{m}_i$, and $\dot{v}_i$ are replaced with ΔP_i, $\dot{M}_{E,i}$, and $\dot{V}_{E,i}$:

$$f_i = \frac{\Delta P_i}{\dot{M}_{E,i} \dot{V}_{E,i}} \frac{2 D_{H,i} A_i^2}{L_i}, \tag{4}$$

where $\dot{V}_{E,i} = \int_{E_i} \vec{V} \cdot \vec{n} dS$. The pressure drop on the Pronghorn domain is computed as follows. First, we select an arbitrary reference pressure P_R. For simplicity we select the arithmetic average of the face-averaged pressures:

$$P_R = \frac{1}{I} \sum_{i=1}^{I} \overline{P}_{E_i}. \tag{5}$$

The choice of P_R ultimately does not matter because it cancels out when pressure drops between system side boundaries E_i are computed. Then we compute ΔP_i by:

$$\Delta P_i = d \left[(\overline{P}_{E_i} - P_R) + (p_{B,i} - p_B) \right]. \tag{6}$$

The second term in the above expression reduces the pressure drop that is imposed in the component by the amount that is present between branch and the branch side of the components because of changes in flow area.

As an example of where the *simple* approach would fail to produce self-consistent pressured drops, consider a pipe filled with an incompressible fluid. At a constant inlet speed of $v = 1$, the pressure drop is given by Δp. At a certain time, the velocity is increased linearly from $v = 1$ to $v = 2$. At the ultimate steady-state, the pressure drop will be $4\Delta p$. However, during the transient the pressure drop across the pipe does not only contain irreversible pressure drops but also the pressure difference necessary to accelerate the mass of the fluid that is in the pipe. This additional pressure drop is given by: $\Delta p_{\text{acc}} = L\rho \frac{dv}{dt}$. When using the *simple* approach, the pressure drop computed by Pronghorn contains Δp_{acc} and not just the steady-state portion of the pressure drop. However, in SAM it is applied as if it only contained the steady-state portion of the pressure drop such that the time dependent pressure drop is double-counted.

For the *simple* strategy in the energy equation, we define the reference enthalpy by:

$$H_R = \frac{1}{I} \sum_{i=1}^{I} \overline{H}_{E,i}. \tag{7}$$

Then the heat source density in the SAM component is computed as:

$$\dot{q}_i = \frac{\dot{m}_{B,i} H_R - \dot{M}_{E,i} \langle H \rangle_{E_i}}{A_i L_i}. \tag{8}$$

Two comments are in order here. First, the sign of the equation (system side E, i is negative) arises from the convention that $\dot{M}_{E,i} < 0$ if E, i is an outflow boundary. Second, we use $\dot{m}_{B,i}$ as the branch mass flow rate. This ensures that in aggregate over all components the $\dot{m}_{B,i} H_R$ term cancels out and enthalpy differences between system side boundaries $\{E, i\}_{i=1,I}$ are consistent between Pronghorn and SAM (at least in steady-state). Similar to the update for pressure, Eq. 8 neglects the time derivative term in the energy equation in both Pronghorn and SAM so that during a fast transient inconsistent results between Pronghorn and SAM will be obtained. For fast transients, the *update* strategy should be used, while Eq. 8 is useful for obtaining steady-state results via a pseudo time stepping approach.

Passively advected scalar variables differ from the energy variable in that they can decay. Pronghorn and SAM define passive scalar variables differently. To be clear on the definition of the passive scalar equation, we state the passive scalar advection equation that all following equations are based on:

$$\frac{\partial \phi}{\partial t} + \nabla \cdot (\vec{v}\phi) - \lambda\phi = S, \tag{9}$$

where λ is the decay constant. The equation used in SAM differs from Eq. 9 in two aspects [8]:

- all ϕ have a ρ multiplied to them, so in order to compute ϕ from what SAM returns as *Postprocessor* values, we need to multiply by density. This is automatically done in the *MultiAppTransfer* implemented for this work.
- the $\lambda\phi$ term has its sign flipped. This means that when providing decay constants to the two codes, decay would be $\lambda > 0$ for SAM, but $\lambda < 0$ for Pronghorn. Currently, the input has to be provided to each code separately leading to the potential of inconsistent input.

The *simple* strategy for advected passive scalars is more complicated than for pressure or energy because decay has to be taken into account. To derive a suitable expression, we start with Eq. 9 and write it for passive scalar k in component i and for steady-state conditions and a single spatial dimension:

$$\frac{\partial}{\partial x}(v_i \phi_{i,k}) + |\lambda_k| \phi_k = s_{i,k}, \tag{10}$$

where without loss of generality we assume that x is oriented from the inlet to the outlet so that $v \geq 0$. For non-incompressible fluids v can vary which complicates the derivation of a simple

formula. We approximate v as a linear function:

$$v(x) = \underbrace{\frac{v_{E,i} + v_{B,i}}{2}}_{\overline{v}_i} + \underbrace{d\frac{v_{E,i} - v_{B,i}}{L_i}}_{v_{x,i}} (x - L_i/2)\,, \tag{11}$$

where $d = 1$ if the flow in the component i is from the branch to the system side and -1 if the flow is from the system side to the branch. The velocities $v_{E,i}$ and $v_{B,i}$ are computed from SAM mass flow rates and densities. Substituting Eq. 11 into Eq. 10 leads to:

$$\overline{v}_i \frac{\partial \phi_{i,k}}{\partial x} + (|\lambda_k| + v_{x,i})\,\phi_k = s_{i,k}. \tag{12}$$

Equation 12 can be solved analytically. The solution is:

$$\phi_{i,k}(L_i) = \phi_{i,k}(0)e^{-\alpha_{i,k}} + \frac{s_{i,k}}{|\lambda_k| + v_{x,i}} \left(1 - e^{-\alpha_{i,k}}\right), \tag{13}$$

where $\phi_i(L_i)$ and $\phi_i(0)$ are the outlet and inlet values of the passive scalars and $\alpha_{i,k} = \frac{(|\lambda_k| + v_{x,i})L_i}{\overline{v}_i}$. We now solve for $s_{i,k}$ and replace the $\phi_i(L_i)$ and $\phi_i(0)$ with the values obtained by the Pronghorn solve:

$$s_{i,k} = \frac{(\langle\Phi_k\rangle(L_i) - \langle\Phi_k\rangle(0)e^{-\alpha})\,(|\lambda_k| + v_{x,i})}{1 - e^{-\alpha}}. \tag{14}$$

For small $\alpha_{i,k}$, we expand Eq. 14 into a Taylor series and obtain:

$$s_{i,k} = \frac{\overline{v}_i}{L_i} \left(\langle\Phi_k\rangle(L_i) - (1 - \alpha_{i,k})\langle\Phi_k\rangle(0)\right), \tag{15}$$

where $\langle\Phi_k\rangle(L_i)$ and $\langle\Phi_k\rangle(0)$ are either $\langle\Phi_k\rangle_{E,i}$ or $\langle\Phi_k\rangle_{B,i}$ depending on the sign of $\dot{M}_i$.

2.6.2 The *update* approach

The idea of the *update* approach is to iterate on the Darcy-Weisbach coefficient $f_i^{(n)}$ until a self-consistent pressure drop between SAM and Pronghorn is achieved. To derive an update formula, we write the SAM pressure drop at iteration n, $\Delta p_i^{(n)} = d(p_{E,i}^{(n)} - p_B^{(n)})$, in terms of SAM mass and volumetric flow rates, the Darcy-Weisbach factor computed by Pronghorn in the last iteration, and

an error term $\eta^{(n)}$:

$$\Delta p_i^{(n)} = \frac{1}{2}\frac{L_i}{D_{H,i}A_i^2} f_i^{(n-1)} \dot{m}_{E,i}\dot{v}_{E,i} + \eta^{(n)}. \tag{16}$$

In the next Pronghorn iteration, the friction factor would be computed using the equation:

$$\Delta P_i^{(n)} \leftarrow \frac{1}{2}\frac{L_i}{D_{H,i}A_i^2} f_i^{(n)} \dot{M}_{E,i}\dot{V}_{E,i}, \tag{17}$$

if the *simple* approach were to be used. However, we know that this equation is not exact and needs to be corrected. We assume that the same error term as in Eq. 16 also corrects this expression:

$$\Delta P_i^{(n)} = \frac{1}{2}\frac{L_i}{D_{H,i}A_i^2} f_i^{(n)} \dot{M}_{E,i}\dot{V}_{E,i} + \eta^{(n)}. \tag{18}$$

We obtain an update formula for the Darcy-Weisbach friction factor by eliminating $\eta^{(n)}$:

$$f_i^{(n)} = \frac{\dot{m}_{E,i}^{(n)}\dot{v}_{E,i}^{(n)}}{\dot{M}_{E,i}^{(n)}\dot{V}_{E,i}^{(n)}} f_i^{(n-1)} + r\frac{\Delta P_i^{(n)} - \Delta p_i^{(n)}}{\frac{1}{2}\frac{L_i}{D_{H,i}A_i^2}\dot{M}_{E,i}^{(n)}\dot{V}_{E,i}^{(n)}}, \tag{19}$$

where r is a user-controlled under-relaxation factor. The update formula for the Darcy-Weisbach friction factor, Eq. 19 usually converges better if Eq. 6 is used up to a point during the transient when the solution has sufficiently stabilized.

We use the idea of an iteratively updated correction to derive an *update* algorithm for the energy equation. The resulting iteration is given by:

$$\begin{aligned}
\dot{H}_i^{(n)} &= \dot{m}_{B,i}^{(n)} H_R^{(n)} - \dot{M}_{E,i}^{(n)} \langle H \rangle_{E_i}^{(n)} \\
\dot{h}_i^{(n)} &= \dot{m}_{B,i}^{(n)} h_{B,i}^{(n)} - \dot{m}_{E,i}^{(n)} h_{E,i}^{(n)} \\
\dot{q}_i^{(n)} &= \dot{q}_i^{(n-1)} + r\frac{\dot{H}_i^{(n)} - \dot{h}_i^{(n)}}{L_i A_i},
\end{aligned} \tag{20}$$

where r can be different from Eq. 19. This iteration converges to a consistent Pronghorn-SAM enthalpy difference measured between system side boundaries; however, convergence is slow. Therefore, we use the following quasi-Newton method instead. We want to find $\dot{q}_i$ such that:

$$\dot{h}_i(\dot{q}_i) - \dot{H}_i = 0. \tag{21}$$

We linearly expand around the current iterate:

$$\dot{h}_i^{(n)} + \left.\frac{d\dot{h}_i}{d\dot{q}_i}\right|^{(n)} \left(\dot{q}_i^{(n+1)} - \dot{q}_i^{(n)}\right) - \dot{H}_i^{(n)} = 0 \tag{22}$$

Solving for $\dot{q}_i^{(n+1)}$ and introducing the relaxation factor r gives:

$$\dot{q}_i^{(n+1)} = \dot{q}_i^{(n)} + r\frac{\dot{H}_i^{(n)} - \dot{h}_i^{(n)}}{\left.\frac{d\dot{h}_i}{d\dot{q}_i}\right|^{(n)}}. \tag{23}$$

The derivative is approximated by:

$$\left.\frac{d\dot{h}_i}{d\dot{q}_i}\right|^{(n)} \approx \frac{\dot{h}_i^{(n)} - \dot{h}_i^{(n-1)}}{\dot{q}_i^{(n)} - \dot{q}_i^{(n-1)}}. \tag{24}$$

During the iteration procedure, we monitor the "health" of the approximation to the derivative (e.g., it cannot be negative and causes issues if it is very small) and switch between Eq. 20 and Eq. 23 as needed.

An *update* equation can be derived for the passive scalars by:

$$\begin{aligned}
\phi_{i,k}(L_i)^{(n)} &= \phi_{i,k}(0)^{(n)} e^{-\alpha_{i,k}^{(n)}} + \frac{s_{i,k}^{(n-1)}}{|\lambda_{i,k}| + v_{x,i}^{(n)}}\left(1 - e^{-\alpha_{i,k}^{(n)}}\right) + C_{i,k}^{(n)} \\
\langle\Phi_k\rangle^{(n)}(L_i) &= \langle\Phi_k\rangle^{(n)}(0) e^{-\alpha_{i,k}^{(n)}} + \frac{s_{i,k}^{(n)}}{|\lambda_{i,k}| + v_{x,i}^{(n)}}\left(1 - e^{-\alpha_{i,k}^{(n)}}\right) + C_{i,k}^{(n)}.
\end{aligned} \tag{25}$$

Eliminating $C_{i,k}^{(n)}$ gives:

$$s_{i,k}^{(n)} = s_{i,k}^{(n-1)} + r\frac{|\lambda_k| + v_{i,x}}{1 - e^{-\alpha_{i,k}^{(n)}}}\left[\left(\langle\Phi_k\rangle^{(n)}(L_i) - \phi_{i,k}(L_i)^{(n)}\right) - e^{-\alpha_{i,k}^{(n)}}\left(\langle\Phi_k\rangle^{(n)}(0) - \phi_{i,k}(0)^{(n)}\right)\right]. \tag{26}$$

For small $\alpha_{i,k}^{(n)}$, we expand Eq. 26 into a Taylor series:

$$s_{i,k}^{(n)} = s_{i,k}^{(n-1)} + r\frac{\overline{v}_i^{(n)}}{L_i}\left[\left(\langle\Phi_k\rangle^{(n)}(L_i) - \phi_{i,k}(L_i)^{(n)}\right) - \left(1 - \alpha_{i,k}^{(n)}\right)\left(\langle\Phi_k\rangle^{(n)}(0) - \phi_{i,k}(0)^{(n)}\right)\right]. \tag{27}$$

Similar to the energy equation, Eq. 26 converges slowly. Therefore, a quasi-Newton method is

implemented. The derivation of this equation is identical to Eq. 23, so only the final result is stated here:

$$s_{i,k}^{(n+1)} = s_{i,k}^{(n)} + r \frac{\left(\langle \Phi_k \rangle^{(n)}(L_i) - \langle \Phi_k \rangle^{(n)}(0)\right) - \left(\phi_{i,k}(L_i)^{(n)} - \phi_{i,k}(0)^{(n)}\right)}{\left.\frac{d\left[\langle \Phi_k \rangle^{(n)}(L_i) - \langle \Phi_k \rangle^{(n)}(0)\right]}{s_{i,k}}\right|^{(n)}}, \tag{28}$$

where the derivative in the denominator is approximated as in Eq. 23.

Consistency between Pronghorn and SAM must be checked for the *update* strategy because it is used as an indication of convergence between Pronghorn and SAM. A convenient way to check consistency is to use the appropriately normalized difference between Pronghorn and SAM which we will refer to as the relative residual in the remainder of the document. The relative residual γ is computed by:

$$\begin{aligned} \gamma^{(n)} &= \frac{1}{\sigma_p^{(n)}} \sum_{i=1}^{I} \left| \Delta p_i^{(n)} - \Delta P_i^{(n)} \right| \\ \text{if energy present: } \gamma &:= \gamma + \frac{1}{\sigma_H^{(n)}} \sum_{i=1}^{I} \left| \dot{h}_i^{(n)} - \dot{H}_i^{(n)} \right| \\ \gamma &:= \gamma + \sum_{k=1}^{K} \frac{1}{\sigma_\phi^{(n)}} \sum_{i=1}^{I} \left| \langle \Phi_k \rangle^{(n)}(L_i) - \phi_{i,k}^{(n)}(L_i) \right|, \end{aligned} \tag{29}$$

where

$$\begin{aligned} \sigma_p^{(n)} &= \frac{1}{I} \sum_{i=1}^{I} \left| \overline{P}_{E,i}^{(n)} \right| \\ \sigma_H^{(n)} &= \frac{1}{I} \sum_{i=1}^{I} \left| \dot{H}_i^{(n)} \right| \\ \sigma_\phi^{(n)} &= \frac{1}{IK} \sum_{k=1}^{K} \sum_{i=1}^{I} \left| \langle \phi_k^{(n)} \rangle_{E_i} \right|. \end{aligned} \tag{30}$$

The MOOSE *MultiApp* system performs the following two checks:

$$\begin{aligned} \gamma^{(n)} &< \text{tol}_{\text{abs}} \\ \gamma^{(n)} / \gamma^{(0)} &< \text{tol}_{\text{rel}}, \end{aligned} \tag{31}$$

and convergence is asserted if one of these conditions is met.

2.7 Code Design

The overlapping domain coupling uses the *MultiApp* system with Pronghorn as main application and SAM as sub application. A custom action syntax currently labeled *[OverlappingDomainCoupling]* sets up all additional objects on the Pronghorn and SAM side and modifies the components on the SAM side. The action behind the *[OverlappingDomainCoupling]* syntax requires the existence of a Navier-Stokes FV action.

A custom *MultiAppTransfer* object *MultiAppOverlapTransfer* performs the information transfers. The computation of source terms in SAM for achieving a self-consistent solution are computed in a custom *UserObject* called *DomainOverlappingUserObject*. A custom *Postprocessor* is implemented to compute mass-flow rate weighted averages on Pronghorn boundaries as well as a custom *Postprocessor* called *OverlapConvergence* that receives the iterative error from the *DomainOverlappingUserObject* at each fixed-point iteration. The *OverlapConvergence Postprocessor* can be used for a custom fixed-point convergence check.

Listing 1 provides the input file syntax for setting up the domain overlapping coupling between Pronghorn and SAM. Most of the simulation is driven by the *OverlappingDomainCoupling* block, but to avoid information duplication, it uses the *NavierStokesFV* action syntax to set common parameter.

```
L_01 = 1
A01 = 0.1
L_02 = 1
A02 = 0.01
L_03 = 1
A03 = 0.1
L_04 = 1
A04 = 0.05
[Modules]
  [NavierStokesFV]
    :
  []
[]
[OverlappingDomainCoupling]
  boundaries = 'bound01 bound02 bound03 bound04'
  component_names = 'pipe01 pipe02 pipe03 pipe04'
  component_orientation = 'in in out out'
  component_area = '${A01} ${A02} ${A03} ${A04}'
  component_length = '${L_01} ${L_02} ${L_03} ${L_04}'
  subapp_filename = 'overlap_thydr_2_sam.i'
  boundary_massflowrate_names = 'pressure_01 pressure_02 pressure_03 pressure_04'
  pinned_pressure_value = 'pinned_pressure_03'
  pinned_pressure_boundary = bound03
  hydrodynamic_iteration_type = update
  overlapped_branch_name = j_01_02_03_04
  startup_time = 1.2
  boundary_pressure_names = ${boundary_pressure_name}
  enthalpy_functor = cp_temp
  thermal_iteration_type = update
  boundary_temperature_names = ${energy_inlet_pps}
  initial_boundary_temperatures = '${T_initial} ${T_initial} ${T_initial} ${
    T_initial}'
  reference_enthalpy = reference_plane_enthalpy
[]
```

Listing 1: Input file snippet of the *OverlappingDomainCoupling* action.

3. Numerical Results

We present three test cases:

- a multi-inlet/multi-outlet test problem with incompressible flow solving for pressure, velocity, and temperature,
- a simple pipe problem with incompressible flow solving for pressure, velocity, and three passive scalar variables,
- a realistic model of the MSRE solving for pressure, velocity, temperature, and 6 passive scalars.

3.1 Multi-inlet/multi-outlet p-v-T test problem

A conceptual sketch of the geometry for this test problem is shown in Fig. 3. The Pronghorn geometry is a two-dimensional double-T junction with two inlets (O1 and O2) and two outlets (O3 and O4). A heat source is placed in the O2 branch of the Pronghorn domain. The overlapped SAM components are indicated in red and are labeled C1-C4. At each boundary, non-overlapped SAM components indicated in black are situated which have either a velocity inlet or pressure outlet boundary condition applied on their far end. The relevant parameters are detailed in Table 1.

The multi-inlet/multi-outlet problem is challenging for overlapping domain decomposition because the temperature at the outlets O3 and O4 depends on how fast the flow through O2 is. If the fluid coming from O2 is faster, the jet at the first T-junction penetrates deeper into the main channel leading to more of the hotter fluid ending up at O3. In addition, the large difference in loss coefficients at the channels right after O3 and O4 makes the pressure at the boundaries O3 and O4 strongly dependent on the mass flow rate distribution between the outlets O3 and O4. Convergence from the naive initial guess of zero velocity when using *update* strategy for both pressure and enthalpy has problem converging. Therefore, we use the *simple* strategy for the first 1.2 seconds of simulation time (i.e., from $t = -1$ to $t = 0.2$ seconds).

Numerical results of the overlapping domain coupling between Pronghorn and SAM are presented in Figs 4 to 9. The temperature and velocity fields in the overlapped portion of the problem are depicted in Fig 4. The fluid in the O2 leg is heated up by the source and by its own

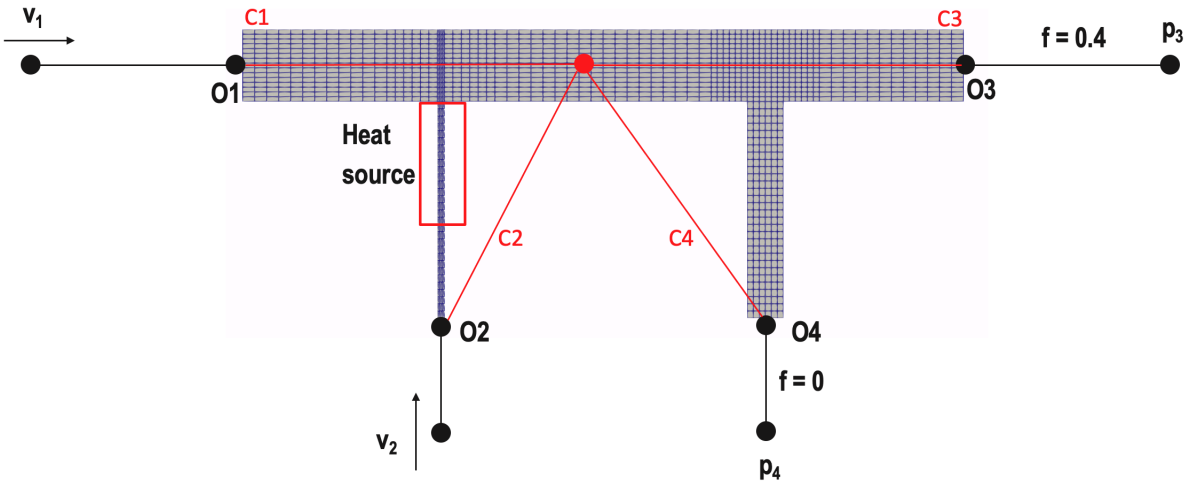

Figure 3: Geometry of the multi-inlet/multi-outlet p-v-T test problem.

Table 1: Parameters for the multi-inlet/multi-outlet p-v-T test problem.

Name	Parameter description
v_1	Initial ramp from 0 to 0.3 m/s from -1 to 0 seconds, Ramp from 0.3 to 0.35 m/s from 3 to 5 seconds
v_2	Initial ramp from 0 to 2 m/s from -1 to 0 seconds, Ramp from 2 to 3m/s from 3 to 5 seconds
p_3, p_4	gauge
Loss coefficient before O1	$f = 0.01$
Loss coefficient before O2	$f = 0.01$
Loss coefficient past O3	$f = 0.4$
Loss coefficient past O4	$f = 0$
Heat source	Linear ramp from 0 to 2×10^9 W/m^3 from 3 to 5 seconds
Fluid density	1000 kg/m^3
Temperature at O1 and O2	300 K
Specific heat	4200 J/kg-K
A_1	0.1 m^2
A_2	0.01 m^2
A_3	0.1 m^2
A_4	0.05 m^2
Transient start time	$t = -1$ seconds
Transient end time	$t = 30$ seconds
Startup time	$t > 0.2$ seconds (Note: duration of 1.2 seconds)

velocity penetrates into the main flow as a jet. The penetration depth of the jet determines the temperature distribution of the fluid after the first T junction. When the flow moves past the second T-junction, the fluid close to the bottom wall is redirected to the O4 exit. Depending on the temperature distribution between the two T-junction more or less heated fluid makes it to the O3 outlet.

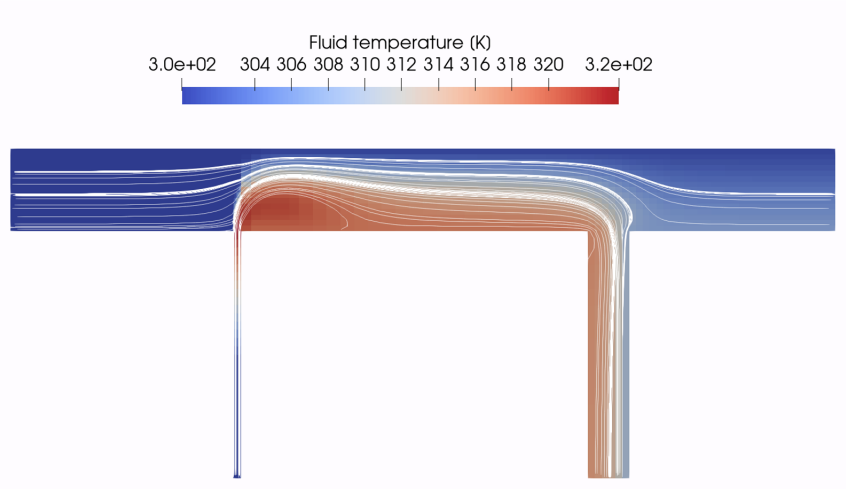

Figure 4: Distribution of temperature and streamlines for the multi-inlet/multi-outlet p-v-T problem at $t = 25$ seconds.

Consistency between the Pronghorn and SAM solutions for the mass flow rate, pressure differences between system side boundaries, and temperatures are depicted in Figs. 5, 6, and 7. These plots show that after switching from the *simple* to the *update* strategy at $t = 0.2$ seconds, mass flow rates at the outlets, pressure differences between system side boundaries, and temperatures at the outlet boundaries are consistent between Pronghorn and SAM. The small discrepancies right before $t = 0.2$ seconds indicate that the *simple* strategy does not produce consistent Pronghorn/SAM solutions during transients.

The relative residual versus number of iterations is plotted for the iteration at $t = 4$ and $t = 7.2$ seconds. In both cases, convergence is achieved after 13 and 6 iterations for $t = 4$ and $t = 7.2$ seconds, respectively; this convergence is rapid when compared to domain-separated coupling. There is a qualitative differences between the reduction in relative residual at $t = 4$ and $t = 7.2$ seconds. At $t = 4$ seconds, we see convergence that is characteristic for a fixed point iteration, namely a reduction by a fixed ratio at each iteration. At $t = 7.2$ seconds, the convergence rate increases as the iteration progresses which is indicative of a Newton or quasi-Newton method.

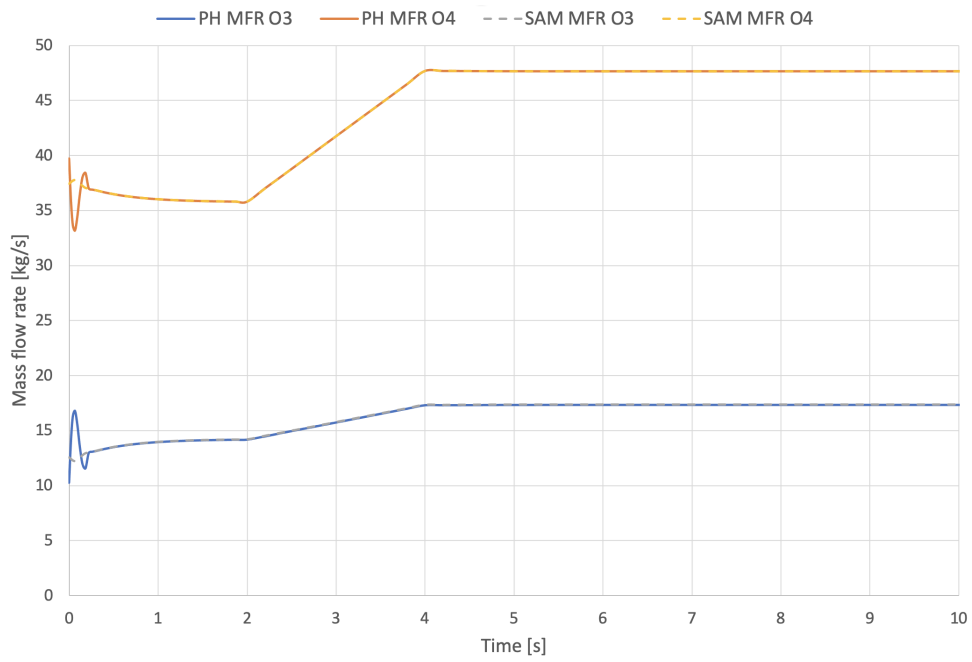

Figure 5: Mass flow rates at the outlets O3 and O4 for Pronghorn (PH) and SAM. The mass flow rates computed by Pronghorn and SAM are identical except for small difference right before the iteration scheme is switched from *simple* to *update*.

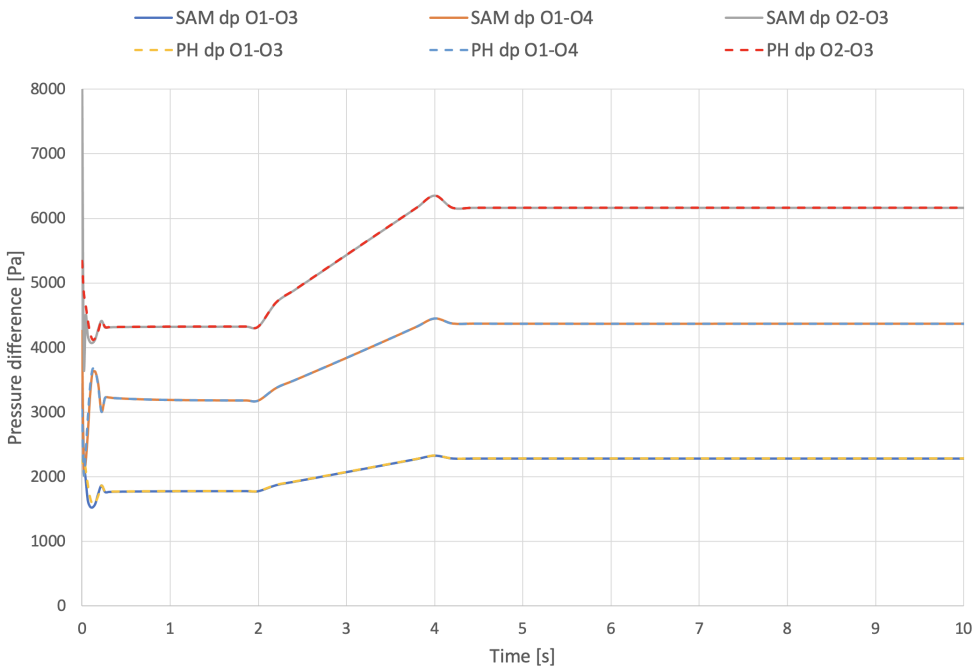

Figure 6: Pressure differences measured between outlets O1-O3, O1-O4, and O2-O3 for Pronghorn (PH) and SAM. For each pair of outlets, the pressure differences computed by Pronghorn and SAM are identical except for small difference right before the iteration scheme is switched from *simple* to *update*.

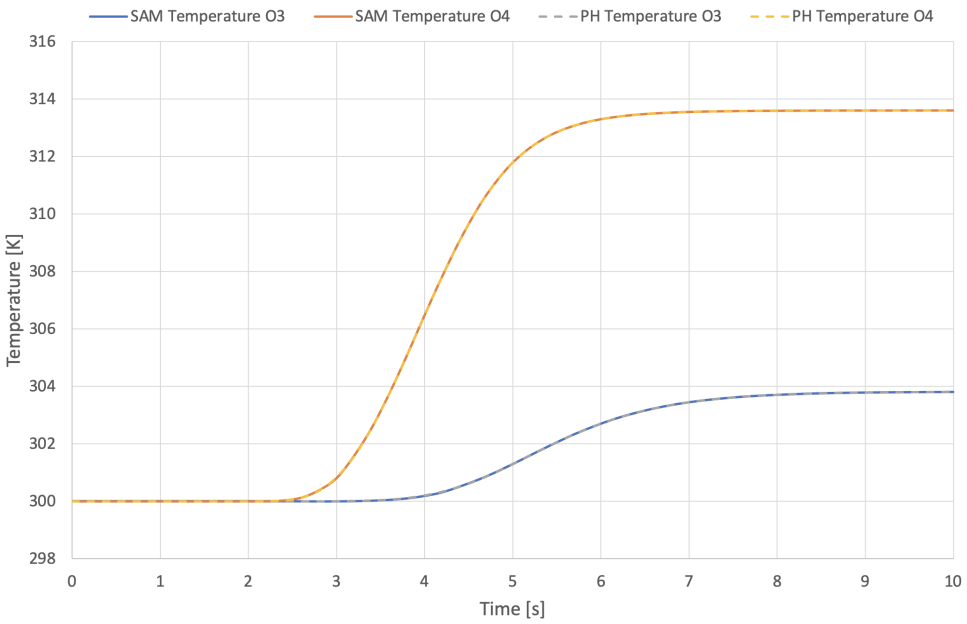

Figure 7: Temperature at the outlets O3 and O4 for Pronghorn (PH) and SAM. The temperatures computed by Pronghorn and SAM are identical.

The differing behavior is caused by using a fixed-point iteration for pressure, but a quasi-Newton method for the energy equation. At $t = 4$ seconds pressure and velocity are not in steady-state yet, so the iteration on pressure limits the convergence rate. However, at $t = 7.2$ seconds, pressure and velocities have reached their steady values so no iteration on Pronghorn/SAM consistency is required.

In Fig. 9, the number of iterations between Pronghorn and SAM to achieve convergence to $\text{tol}_{\text{abs}} = \text{tol}_{\text{rel}} = 10^{-6}$ is depicted. For most of the transient fewer than 10 iterations are required. However, early in the transient $10 - 15$ iterations are required for convergence. The results in Fig. 8 suggests that the slower convergence of the pressure-velocity consistency are responsible for the comparatively slow convergence rates. It may therefore be beneficial to use a quasi-Newton method for the iteration on pressure consistency as well.

3.2 Simple pipe flow with decaying passive scalars

The geometry of this test problem consists of an overlapped two-dimensional flow channel with flow area of 1 meter and length of 10 meters. The SAM model consists of two overlapped flow channel connected at a common branch and two flow channels at either end of the overlapped

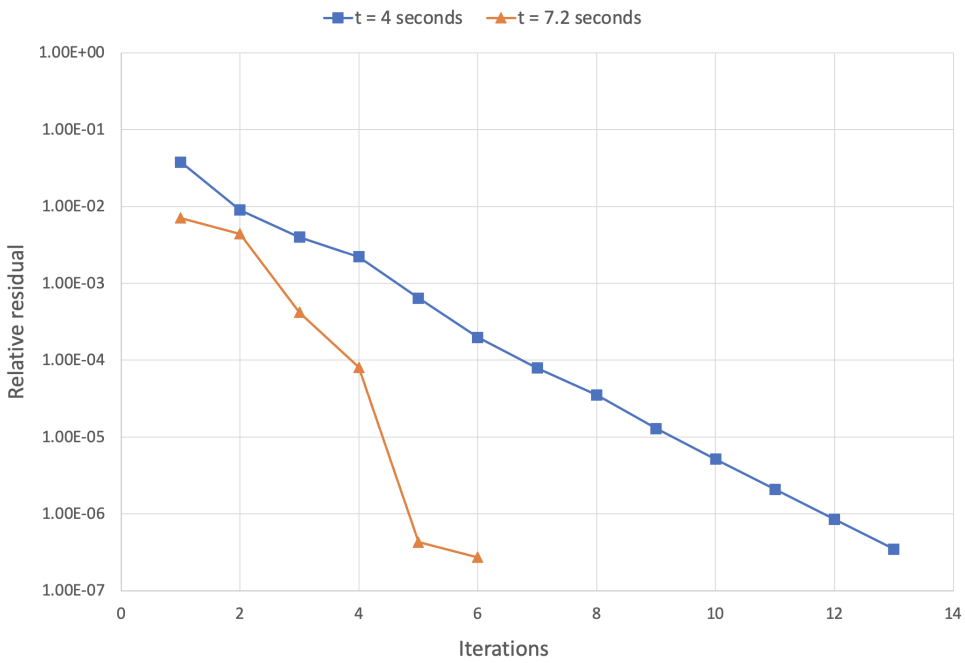

Figure 8: Relative residual for the *update* scheme between Pronghorn and SAM at $t = 4$ and $t = 7.2$ seconds.

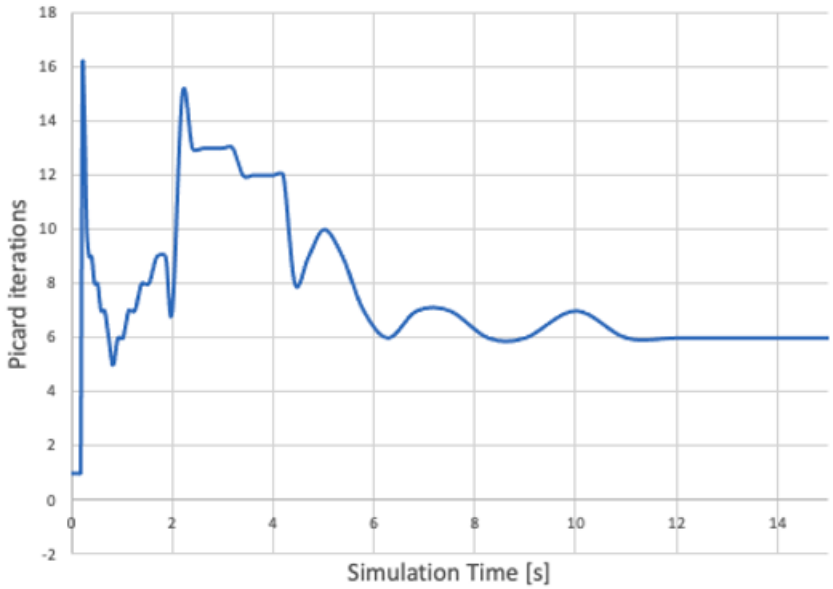

Figure 9: Number of iterations required to meet $\text{tol}_{\text{abs}} = \text{tol}_{\text{rel}} = 10^{-6}$.

Table 2: Passive scalar parameters for the simple pipe flow problem.

Passive scalar	λ [1/s]	Inlet concentration	Source[1]
ϕ_1	1	$0.5\left(1+\cos\left(\frac{2\pi t}{25}\right)\right)$	10
ϕ_2	0.1	$2\left(1-\cos\left(\frac{2\pi t}{12.2}\right)\right)$	$5\,(x+5)\sin\left(\frac{2\pi t}{5}\right)$
ϕ_3	0	$8\left(1-\cos\left(\frac{2\pi t}{400}\right)\right)$	$5\,(x+5)\sin\left(\frac{2\pi t}{50}\right)$
ϕ_4	0	$8\left(1-\cos\left(\frac{2\pi t}{12.2}\right)\right)$	$5\,(x+5)\sin\left(\frac{2\pi t}{200}\right)$

[1] Left edge at $x = 0$

region; all flow channels have the same area. The flow is incompressible ($\rho = 1000$) and isothermal ($T = 300$ K). The inlet velocity is ramped from 0 to 0.5 m/s from $t = 0$ to $t = 1$ seconds and then ramped from 0.5 m/s to 1.2 m/s from $t = 2$ to $t = 4$ seconds. Four passive scalars are advected with the flow. The specifications for these passive scalars are detailed in Table 2. The oscillation of the inlet conditions, source terms, together with the transit time creates challenging time dependence of the passive scalar value concentration at the outlet. The simulation starts at $t = 0$ seconds and iteration strategy switches from *simple* to *update* at $t = 1.2$ seconds.

The concentration of the passive scalars 1 through 4 at the outlet of the overlapped domain as a function of time computed by Pronghorn and SAM are depicted in Fig. 10. After $t = 1.2$ seconds, Pronghorn and SAM compute consistent outlet passive scalar concentrations. Before switching to the *update* strategy, Pronghorn and SAM computed values are not consistent. In particular, for passive scalar 1 the values differ significantly, while the discrepancies are much smaller for passive scalars 2-4.

3.3 Molten salt reactor experiment

The molten salt reactor experiment (MSRE) was an experimental nuclear reactor that operated at Oak Ridge National Laboratory (ORNL) in the United States from 1965 to 1969. It was a pioneering project that aimed to demonstrate the feasibility of using molten salt as both coolant and fuel medium. The MSRE utilized a eutectic mixture of lithium fluoride (LiF) and beryllium fluoride (BeF2), which served as both the fuel carrier salt and the coolant. The primary fuel in the MSRE was uranium-235, which was dissolved in the molten salt. The fuel was circulated through the reactor core, where most of the nuclear fission reactions occurred.

The main technical features of the MSRE included:

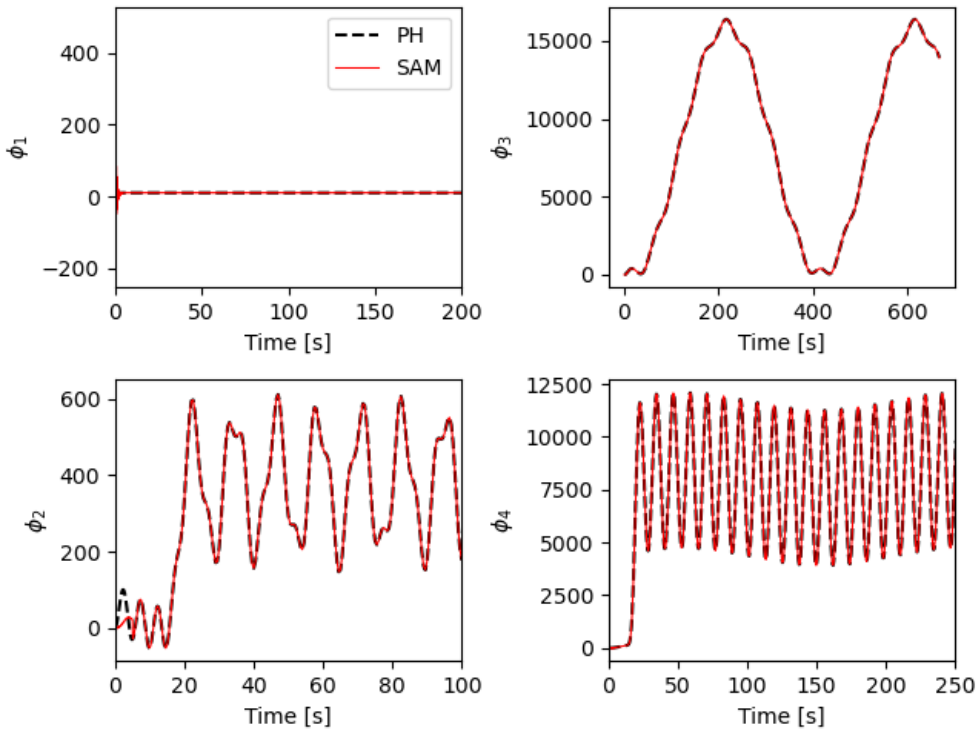

Figure 10: Concentration of the passive scalars 1 through 4 at the outlet of the overlapped domain computed by Pronghorn and SAM.

1. Fuel circulation system: The reactor core contained channels in the graphite moderator that acted as fuel and coolant passages. The fuel salt was continuously circulated through the core using electromagnetic pumps, which facilitated heat transfer and the removal of fission products.

2. Graphite moderator: Graphite was used as a moderator to slow down neutrons, promoting a sustained nuclear chain reaction. The core was surrounded by a graphite reflector to enhance neutron economy.

3. Two-loop heat exchange system: The reactor included a circulating fuel circuit that was cooled down by an external heat exchanger, the loop circulation time in the reactor was $\sim$ 25s.

4. Safety features: The MSRE was designed with inherent safety features, such as highly negative reactivity feedback with respect to temperature. These features allowed engineers to safely perform reactivity insertion transients, among other experiments.

The MSRE was built in 1964 at ORNL to be the first reactor designed and operated with liquid fuel and moderated with graphite. MSRE has a thermal spectrum that is attained by neutron moderation in a graphite block. The coolant/fuel flows through channels in the graphite block. The reactor was initially operated with U-235 fuel, which was later replaced with U-233 fuel. The main reactor specifications are presented in Table 3.

Table 3: MSRE Reactor Specifications

Parameter	Value
Core Power [MW_{th}]	10
Core height [m]	1.63
Core diameter [m]	1.39
Fuel Salt	LiF-BeF_2-ZrF_4-UF_4
Fuel salt molar mass	65.0%-29.1%-5.0%-0.9%
Fuel salt enrichment	33.0%

The MSRE lattice is made of vertical graphite stringers with a cross section of 5.08 cm $\times$ 5.08 cm. The fuel salt flows through a rectangular channel (3.05 cm $\times$ 1.016 cm) with round corners of radius 0.508 cm in the sides of the stringers [13–16]. The core configuration is shown in Figure 11, where the left figure illustrates the layout of MSRE primary and secondary systems [15], and the right figure shows the MSRE reactor assembly [16].

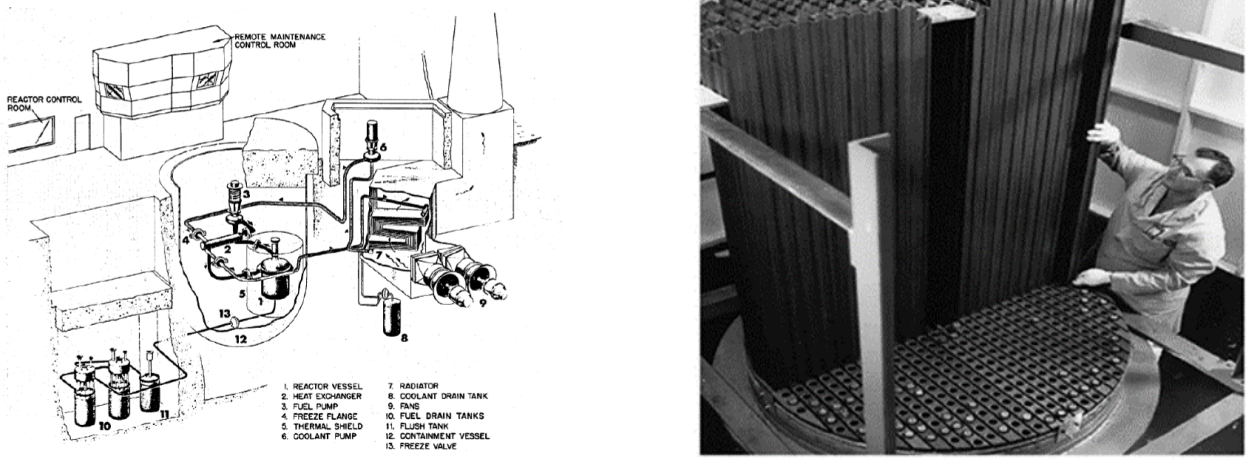

(a) Schematic design of MSRE loops.

(b) Picture of MSRE core graphite stringer.

Figure 11: Configuration of MSRE

In MSRE the core and primary circuit physics strongly interact making it a good example

case for the overlapping domain coupling between Pronghorn and SAM. The core conditions (i.e., temperature and precursor concentrations) determine the fission rate distribution. The fission rate distribution in turn determines the change in temperature and precursor concentrations in the core. The core conditions feed the inlet conditions for the primary circuit where a negligible amount of fission happens, but decay of precursors and cooling (via the heat exchanger) takes place. The outlet conditions for the primary circuit are the inlet conditions for the temperature and precursors at the core inlet. Thus core and primary circuit are coupled via thermal and neutronic feedbacks. The neutronics model for MSRE was taken from [17]. Although this model is quite simplified (e.g., it does not include the control rods and may overestimate leakage at the reactor boundaries), it provides a reasonable power and fission source to estimate the reactor dynamics. We refer the reader to the report [17] for more details about the neutronics model developed in Griffin.

The Pronghorn model of the core is depicted in Figure 12. The model is axisymmetric with the axis being in the vertical direction at the left side of the figure. In the flow loop direction, the model includes the downcomer, lower plenum, core, upper plenum, and top outlet pipe. Between the core and the downcomer, the solid core barrel is included. The core barrel also extends between the upper plenum and the downcomer. Conjugate heat transfer is modeled between the core, upper plenum, and downcomer with the core barrel.

A few key fields describing the core model in Pronghorn during steady-state operation are presented in Figure 13. Firstly, the porosity is 1 everywhere, except for the core, which has a porosity of 0.22283. The porosity of the core is calculated as the flow area between the graphite stringers divided by the total area of the core. It should be noted that the approximation of porosity to be 1 is only approximately true for the downcomer, upper plenum, and outlet pipe. For example, the lower plenum has director baffles that cause the porosity to deviate from 1 and introduce specific pressure drop coefficients. Detailed models of mixing in the lower plenum via high-fidelity calculations are currently being developed in the NEAMS program. For now, we accept the approximation for the lower plenum as it does not affect the demonstration of the domain overlapping coupling between Pronghorn and SAM.

The normalized power source computed by Griffin and passed into Pronghorn is presented in the top panel of Figure 13. The Griffin calculation solely takes into account the lower plenum,

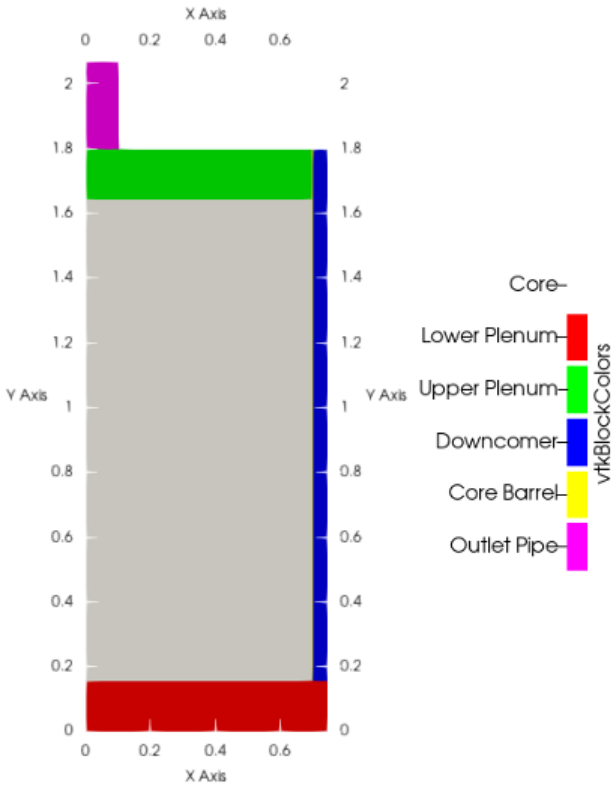

Figure 12: Pronghorn model of MSRE core.

core, and upper plenum. The neutronics in the downcomer and outlet pipe are not considered due to the lack of a detailed model of the core barrel or top dome of the MSRE, which may lead to potentially erroneous results in these regions. Future versions of the Griffin neutronics model will likely include these components. As expected, the power source is larger towards the center of the reactor core. The maximum power source is slightly shifted downwards due to the higher reactivity of the lower temperatures present towards the inlet of the reactor core. The power deposited in the lower and upper plenum represents approximately 15% of the total reactor power.

Lastly, the velocity field during steady-state operation is depicted in the bottom panel of Figure 13. The flow goes downward in the lower plenum, bends and mixes as it enters the core, rises in the core, and finally contracts and mixes in the upper plenum before exiting towards the outlet pipe. The flow is approximately one-dimensional in the core and downcomer due to significantly higher friction factors in the direction perpendicular to the vertical direction. The Churchill-Darcy friction factors [18] are used to compute the pressure drop in the core and

downcomer. The characteristic hydraulic diameter for computing the pressure drop is 1.9133 cm for the core and 51.2701 cm for the downcomer, respectively. No rugosity is assumed when computing the friction factor.

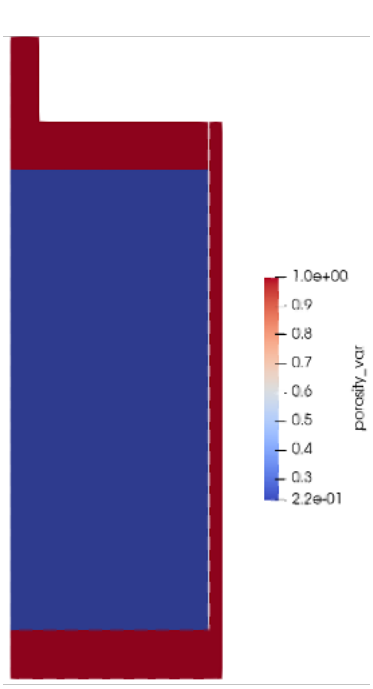

(a) Porosity.

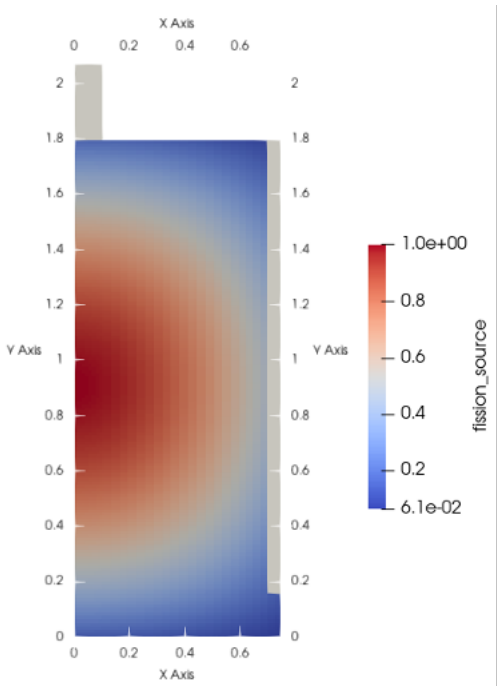

(b) Normalized power source.

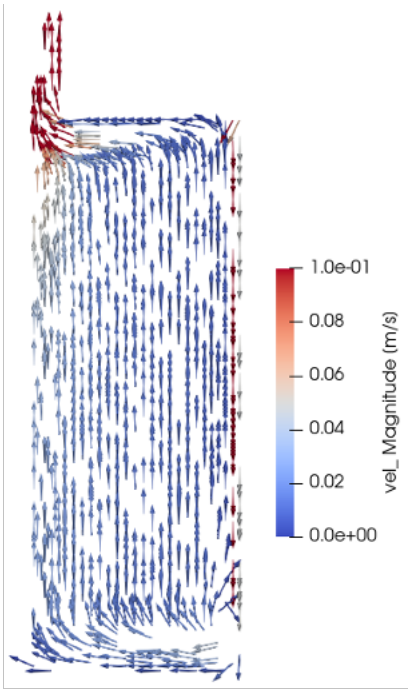

(c) Picture of MSRE core graphite stringer.

Figure 13: Vector plot of the velocity field colored with the velocity magnitude.

The SAM model of the reactor primary loop and heat exchanger system is illustrated in Figure 18. The core, lower plenum, and upper plenum are combined into a single pipe component. The flow in this pipe moves upward, enters the core's outlet pipe, and then proceeds through the pump intake line. Subsequently, the pressure increases as the flow is propelled into the pump's outlet line and then into the primary side of the heat exchanger. Finally, the flow exits the heat exchanger, enters the downcomer through the admission line, and reaches the downcomer. The downcomer and the core and plenum components are connected via a junction in the model.

For the secondary loop, on the shell side of the heat exchanger, the flow enters the heat exchanger through an inlet pipe and exits through an outlet pipe. The inlet and outlet pipes are connected via a central tube. This modeling of the secondary side encompasses the inlet and outlet heat exchanges that occur on the shell side of a shell-and-tube heat exchanger. The heat structures separating the primary and secondary sides are explicitly considered in the model.

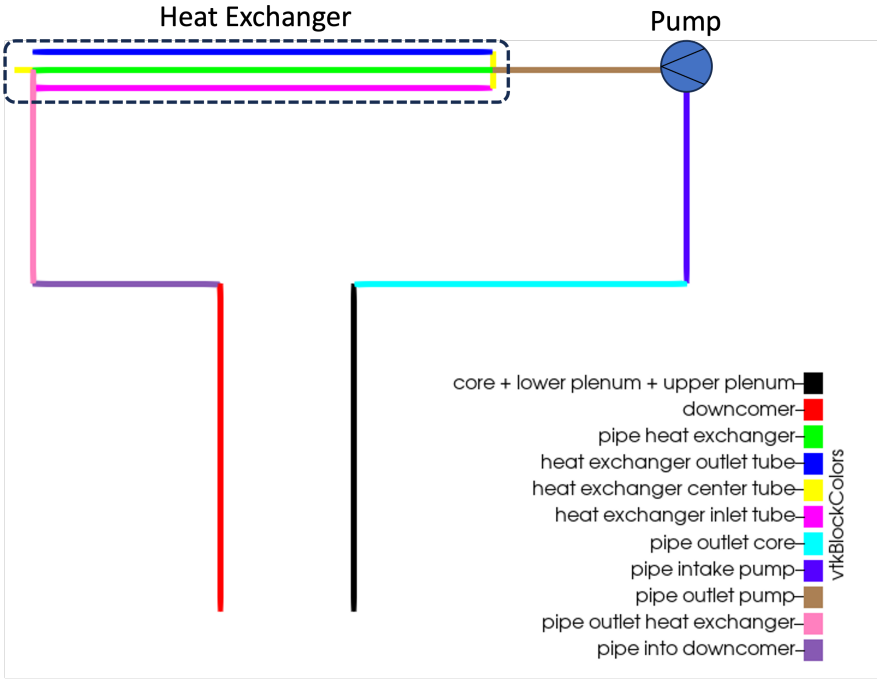

Figure 14: SAM model of MSRE primary circuit and secondary coolant.

The SAM model provides several key results for the steady-state operation, which are depicted in Figure 15. In the top-left panel, the temperature field is presented. As the nuclear power heats the upward circulating flow, the temperature rises in the core and plenum components.

It then remains relatively constant up to the heat exchanger, where heat is transferred to the secondary side. The exit temperature in the heat exchanger is maintained as the flow proceeds to the downcomer and within the downcomer itself.

The density field during operation is shown in the top-right panel of Figure 15. The density of the salt is approximated as a function of temperature only, resulting in higher densities in the colder regions of the primary loop. This density difference generates a buoyancy force in the SAM model.

Furthermore, the heat exchange coefficients at the heat exchanger are depicted in the bottom-left and bottom-right panels of Figure 15 for the primary and secondary sides, respectively. As expected, the heat exchange coefficient is smaller for the primary salt flow compared to the higher-speed forced circulation in the secondary side.

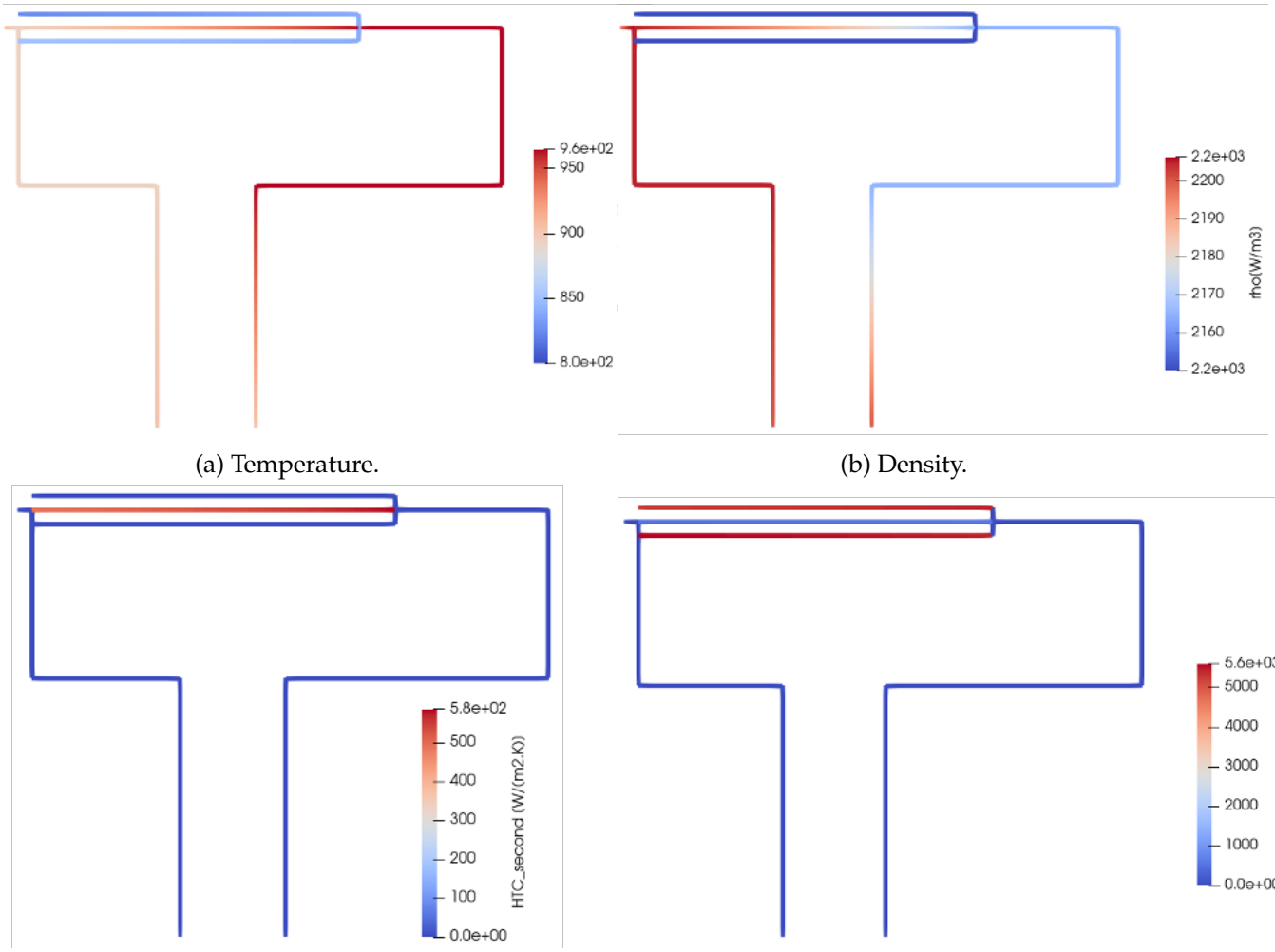

(a) Temperature.

(b) Density.

(c) Heat exchange coefficient on the primary side.

(d) Heat exchange coefficient on the secondary side.

Figure 15: SAM results for steady-state primary circuit and secondary cooling of MSRE.

The coupling between the Pronghorn and SAM models is achieved through the domain overlapping approach. The overlapped domains include the downcomer and the core and plena. Specifically, the downcomer pipe in the SAM model is overlapped with the corresponding downcomer region in the Pronghorn model. Similarly, the pipe representing the core and plena in the SAM model overlaps with the bottom plenum, core, and upper plenum regions in the Pronghorn model. It's important to note that the outlet pipe in the Pronghorn model is not included in the domain-overlap coupling. However, its presence in the Pronghorn model is necessary to accurately represent the flow distribution, pressure drop, and temperature mixing in the top plenum.

The results for the steady-state operation of the MSRE are presented in Figure 17. The top panel

displays the temperature field in both the Pronghorn and overlapped SAM models. The domain overlapping approach incorporates a heat source computed by Pronghorn into the overlapped SAM components. As expected, the heat source in the downcomer, which is solely provided by conjugate heat transfer with the core barrel, is small, resulting in an approximately constant temperature in the downcomer. In the core, the linear heat source computed by Pronghorn leads to a temperature rise in the SAM component that closely follows the temperature predicted by Pronghorn. This can be observed by noting that the temperature predicted in the SAM core and plena component axially is approximately the radial average of the Pronghorn temperature field. Consistent with the methodology implemented in the domain overlapping, the mass-flow-average temperature predicted by Pronghorn at the exit of the core matches the one predicted by SAM.

The bottom panel of Figure 17 presents the velocity field. As expected, the velocities predicted in the SAM coupled components correspond to the radial mass-flow-average of those predicted by Pronghorn. Lastly, it's worth noting that the acceleration in the outlet pipe predicted by the Pronghorn model closely matches the velocity obtained in the outlet pipe of the SAM model, despite these geometries not being included in the coupling. This is attributed to the mass continuity between Pronghorn and SAM during the iterations of the domain overlapping approach, which ensures the same mass flow rate between the two models.

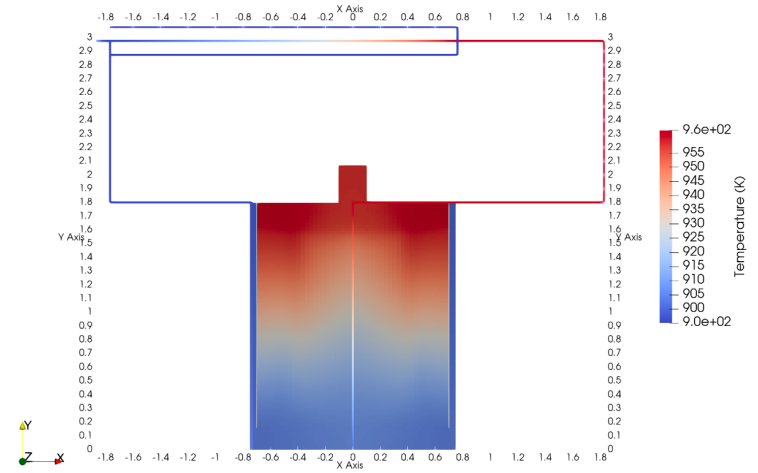

(a) Temperature.

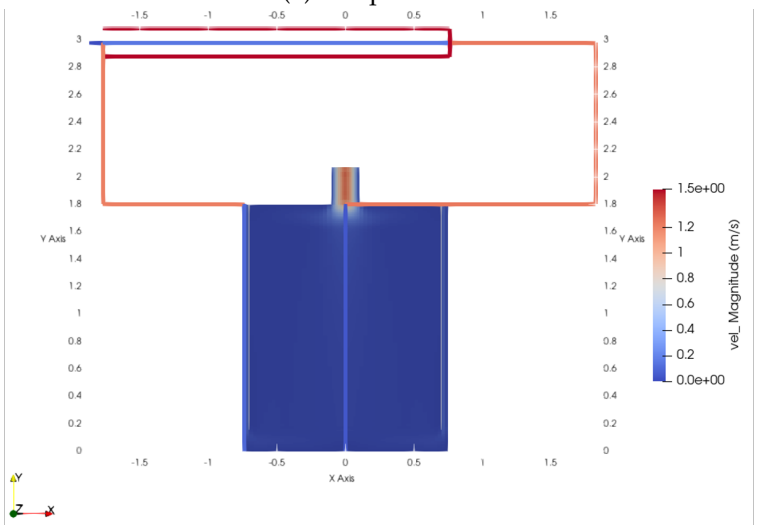

(b) Velocity.

Figure 16: Coupled Pronghorn-SAM thermal-hydraulics results for steady-state primary circuit and secondary cooling of MSRE.

The previous analysis demonstrates the effectiveness of the domain overlapping coupling for the energy and momentum systems. The coupling for the passive scalar system, specifically for the delayed neutron precursors, is shown in Figure 17. Instead of displaying the entire neutron precursor distribution, the figure focuses on three distributions: the longest-lived precursor group (c_1), the shortest-lived precursor group (c_6), and an intermediate group (c_3).

For the longest-lived precursor group (c_1), it is noteworthy that the concentration predicted at the exit of the upper plenum by both Pronghorn and SAM is identical. This demonstrates the accuracy of the precursor source computed by Pronghorn and incorporated into SAM.

Additionally, due to the long lifetime of these neutron precursors, some of them circulate through the primary loop and return to the downcomer. The concentration at the inlet of the downcomer, as predicted by Pronghorn, matches the concentration predicted by SAM, further affirming the successful SAM-to-Pronghorn coupling for passive scalars.

Moving on to the shortest-lived species (c_3 and c_6), it can be observed that the concentrations predicted at the upper plenum by SAMare equal to the average concentrations predicted by Pronghorn to convergence tolerance. Given the rapid decay of these delayed neutron precursors, very little concentration returns to the downcomer. However, an interesting effect associated with these shorter-lived precursors becomes apparent. As their concentrations are small due to their rapid decay, the model predicts a non-negligible concentration of precursors in the downcomer due to turbulent diffusion, which is comparable to the core concentration. Thanks to the precursor source computed by Pronghorn in the downcomer, the SAM model captures this rise of precursors in the downcomer, further highlighting the flexibility of the domain overlapping approach.

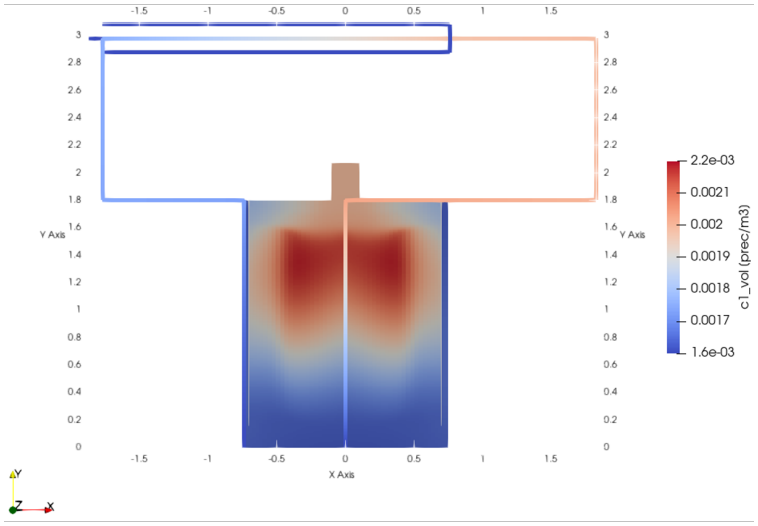

(a) c_1 - Decay Constant = $0.013336 \frac{1}{\text{s}}$.

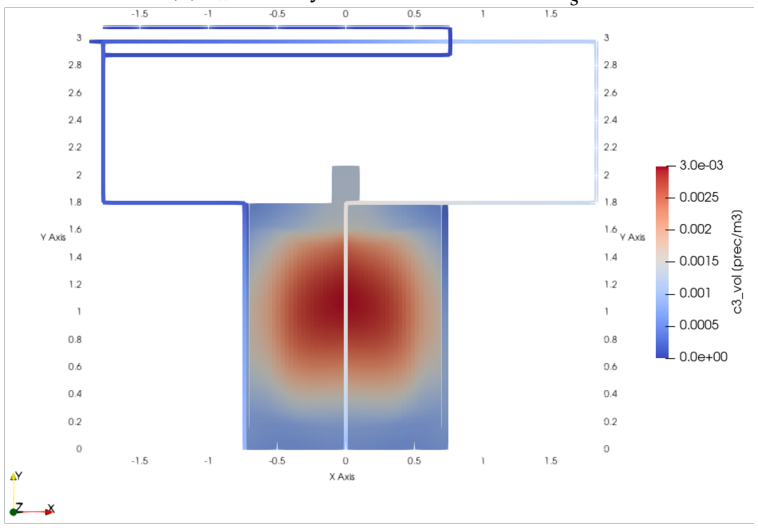

(b) c_3 - Decay Constant = $0.1208 \frac{1}{\text{s}}$.

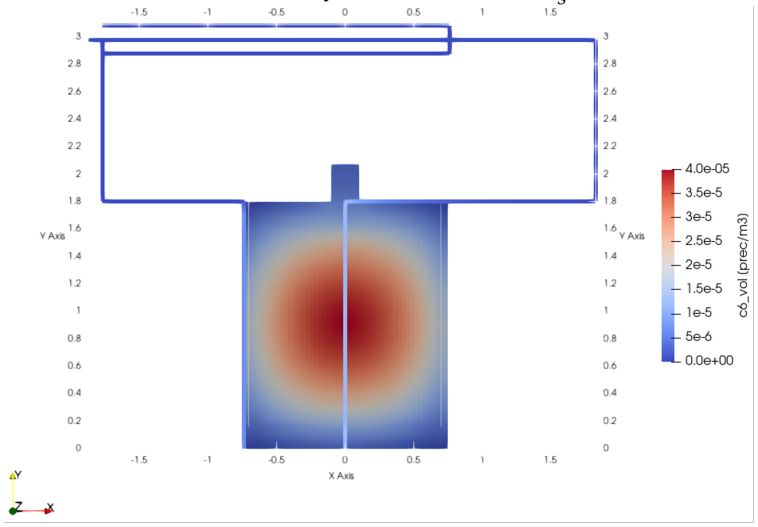

(c) c_6 - Decay Constant = $2.8530 \frac{1}{\text{s}}$.

Figure 17: Coupled Pronghorn-SAM normalized neutron precursors concentration results for steady-state primary circuit of MSRE.

Finally, the domain overlapping approach is applied to simulate the reactivity insertion transient at 5 MW of power in the MSRE. In this transient, the reactor is operating at 5 MW of power when a sudden positive reactivity insertion occurs. Detailed information about the transient and measured data can be found in the ORNL reports [19, 20]. The computed reactivity insertion for the transient was 19 pcm. In the Griffin model, since no control rods are considered, the reactivity insertion is achieved by artificially increasing the fission cross-section of the fuel, resulting in a k-eigenvalue problem with a reactivity 19 pcm higher than the original one. Three models are compared for the reactivity transient:

- The standalone SAM model as documented in INL's Virtual Test Bed [21].
- Domain-segregated coupling between SAM and Pronghorn, where mass flow rates, temperatures, and delayed neutron precursor concentrations are exchanged between SAM and Pronghorn at the boundaries of the upper plenum and downcomer. This approach has been previously documented [10].
- The domain overlapping approach described in this report.

Preliminary results of the power evolution over time are depicted in Figure 18. Immediately after the reactivity insertion, the power in the reactor increases, leading to a temperature rise in the core. This temperature rise, however, reduces the power due to the density-Doppler effect. Subsequently, when the reactor reaches a power level that would result in a steady-state temperature field compensating for the reactivity insertion, the reactor temperature is still higher than the steady-state temperature due to the thermal inertia of the fuel salt. This causes a further reduction in power beyond the equilibrium value, leading to a decrease in temperature, which in turn increases the reactivity. These thermal oscillations in the reactor are accurately captured by all three models. For the initial peak in reactivity, the models integrating Pronghorn exhibit closer agreement with the data. This is mainly due to the multidimensional temperature resolution in the core, which improves the accuracy in capturing the reactivity feedback.

Another observed effect in reactor power is caused by the behavior of neutron precursors, which oscillate in and out of the reactor core, resulting in reactivity swings with a time constant similar to the circulation time of approximately 25 seconds. The 1D SAM model alone is unable

to capture these effects since the neutron precursors rapidly diffuse throughout the core in 1D models. The models integrating Pronghorn, on the other hand, can accurately capture these effects as they are capable of resolving the distribution of neutron precursors in the reactor core, thus limiting artificial smoothing. However, in the case of the domain-segregated approach, there is some loss of information in the interface transfers, leading to an artificial smoothing of neutron precursors. These factors contribute to the superior performance of the domain overlapping approach in this test case. Additionally, this test case serves as further verification for the implemented domain overlapping approach.

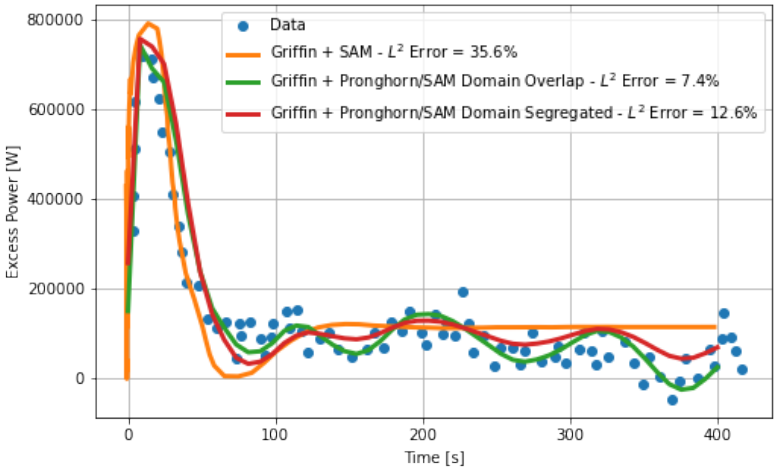

Figure 18: Griffin coupled to thermal-hydraulics model results for reactivity insertion transient at 5MW for MSRE.

4. Summary

A domain-overlapping coupling algorithm between Pronghorn and SAM was developed and implemented into MOOSE. The overlapped SAM components are set up in a sufficiently flexible arrangement to support all relevant geometries: one "overlapped" component for each boundary and all "overlapped" components connected to a single branch. Volumetric terms in the components (friction factors, heat source, and passive scalar source) are automatically updated by Pronghorn in the SAM model within a fixed point or quasi-Newton iteration until consistency is achieved. Simplistically, consistency is understood as having the same averaged pressures, mass flow rates, enthalpies, and passive scalar values in SAM and Pronghorn at each boundary. Two schemes for setting the volumetric terms in SAM are introduced, *simple* and *update*. For the *simple* approach, no iterations between Pronghorn and SAM are performed and the values of the volumetric terms is set by values computed in Pronghorn. For the *update* approach, a fixed point or quasi-Newton iteration on the value the volumetric sources is performed that achieves consistent solutions in about 10 iterations.

We tested the algorithm for three problems: a multi-inlet/multi-outlet pressure-velocity-temperature problem, a simple pipe with four passively advected scalar variables subject to boundary conditions and sources that oscillate with different frequencies, and MSRE. We find that for all test problems, the *update* approach provides consistent Pronghorn-SAM solutions within a reasonable number of iterations.

The following features were tested in this work:

- Numerically stable for a wide range of typical problems.
- Reasonably fast convergence of the fixed-point iterations between Pronghorn and SAM.
- Support multiple boundaries (i.e. more than 2) on the Pronghorn domain.
- Support an arbitrary number of passively advected scalar variables.

The following items must either be implemented or have not been tested yet:

- Allow reversal of flow over boundaries (i.e., an inlet becomes an outlet or vice versa).
- Support compressible fluids.

- Support natural circulation.

REFERENCES

[1] A. J. Novak, R. W. Carlsen, S. Schunert, P. Balestra, D. Reger, R. N. Slaybaugh, and R. C. Martineau, "Pronghorn: A multidimensional coarse-mesh application for advanced reactor thermal hydraulics," *Nuclear Technology*, vol. 207, no. 7, pp. 1015–1046, 2021.

[2] A. D. Lindsay, D. R. Gaston, C. J. Permann, J. M. Miller, D. Andrš, A. E. Slaughter, F. Kong, J. Hansel, R. W. Carlsen, C. Icenhour, L. Harbour, G. L. Giudicelli, R. H. Stogner, P. German, J. Badger, S. Biswas, L. Chapuis, C. Green, J. Hales, T. Hu, W. Jiang, Y. S. Jung, C. Matthews, Y. Miao, A. Novak, J. W. Peterson, Z. M. Prince, A. Rovinelli, S. Schunert, D. Schwen, B. W. Spencer, S. Veeraraghavan, A. Recuero, D. Yushu, Y. Wang, A. Wilkins, and C. Wong, "2.0 - MOOSE: Enabling massively parallel multiphysics simulation," *SoftwareX*, vol. 20, p. 101202, 2022.

[3] C. Fiorina, I. Clifford, M. Aufiero, and K. Mikityuk, "Gen-foam: a novel openfoam® based multi-physics solver for 2d/3d transient analysis of nuclear reactors," *Nuclear Engineering and Design*, vol. 294, pp. 24–37, 2015.

[4] A. Moorthi, A. K. Sharma, and K. Velusamy, "A review of sub-channel thermal hydraulic codes for nuclear reactor core and future directions," *Nuclear Engineering and Design*, vol. 332, pp. 329–344, 2018.

[5] V. Kyriakopoulos, M. E. Tano, and J. C. Ragusa, "Development of a single-phase, transient, subchannel code, within the moose multi-physics computational framework," *Energies*, vol. 15, no. 11, p. 3948, 2022.

[6] V. Kyriakopoulos, M. E. Tano, and A. Karahan, "Demonstration of pronghorn's subchannel code modeling of liquid-metal reactors and validation in normal operation conditions and blockage scenarios," *Energies*, vol. 16, no. 6, p. 2592, 2023.

[7] G. Giudicelli *et al.*, "Coupled multiphysics transient simulations of the mk1-fhr reactor using the finite volume capabilities of the moose framework," in *Mathematics and Computation for Nuclear Science and Engineering*, American Nuclear Society, 2021.

[8] R. Hu, L. Zou, G. Hu, D. Nunez, T. Mui, and T. Fei, "Sam theory manual,"

[9] D. R. Gaston, C. J. Permann, J. W. Peterson, A. E. Slaughter, D. Andrš, Y. Wang, M. P. Short, D. M. Perez, M. R. Tonks, J. Ortensi, L. Zou, and R. C. Martineau, "Physics-based multiscale coupling for full core nuclear reactor simulation," *Annals of Nuclear Energy*, vol. 84, pp. 45–54, 2015.

[10] R. Hu, J. Fang, D. Nunez, M. Tano, G. Giudicelli, and R. Salko, "Development of integrated thermal fluids modeling capability for msrs,"

[11] A. Huxford, V. Petrov, A. Manera, V. C. Leite, E. Merzari, and L. Zou, "Development of innovative overlapping-domain coupling between sam and nekrs," in *Proceedings of NURETH*, 2022.

[12] A. Huxford, V. C. Leite, E. Merzari, L. Zou, V. Petrov, and A. Manera, "A hybrid domain overlapping method for coupling system thermal hydraulics and cfd codes," *Annals of Nuclear Energy*, vol. 189, p. 109842, 2023.

[13] M. Rosenthal, P. Kasten, and R. Briggs, "Molten-salt reactors—history, status, and potential," *Nuclear Applications and Technology*, vol. 8, no. 2, pp. 107–117, 1970.

[14] P. N. Haubenreich and J. Engel, "Experience with the molten-salt reactor experiment," *Nuclear Applications and technology*, vol. 8, no. 2, pp. 118–136, 1970.

[15] R. Robertson, "Msre design and operations report, part i, description of reactor design," *Oak Ridge National Laboratory*, vol. ORNL-TM-728, 1965.

[16] R. Briggs, "Molten-salt reactor program semiannual progress report," *Oak Ridge National Laboratory*, vol. ORNL-3626, 1964.

[17] M. Jaradat and J. Ortensi, "Thermal spectrum molten salt-fueled reactor reference plant model," *Idaho National Laboratory*, vol. INL/RPT-23-72875, 07 2023.

[18] S. W. Churchill, "Friction-factor equation spans all fluid-flow regimes.," 1977.

[19] R. Steffy and P. Wood, "Theoretical dynamic analysis of the msre with 233u fuel," *ORNL-TM-2571*, 1969.

[20] R. Steffy Jr, "Experimental dynamic analysis of the msre with 233u fuel, ornl-tm-2997," *Oak Ridge National Laboratory.*, 1970.

[21] R. Hu *et al.*, "Fy21 sam developments for msr modeling.," Tech. Rep. ANL/NSE-21/74, Argonne National Laboratory, 2021.